Nonlinear Processes in Geophysics (1999) 6: 51–65

Nonlinear Processes in Geophysics

Nonlinear analysis of magnetospheric data Part I. Geometric characteristics of the AE index time series and comparison with nonlinear surrogate data

G. P. Pavlos[1], M. A. Athanasiu[1], D. Kugiumtzis[2], N. Hatzigeorgiu[3], A. G. Rigas[1] and E. T. Sarris[1]

[1]Department of Electrical and Computer Engineering, Demokritos University of Thrace, 67100 Xanthi, Greece
[2]Max-Plank Institute for Physics of Complex Systems, 01187 Dresden, Germany
[3]Institute for Language and Speech Processing, Xanthi Branch, Greece

Received: 09 January 1999 – Accepted: 17 April 1999

Abstract. A long AE index time series is used as a crucial magnetospheric quantity in order to study the underlying dynamics. For this purpose we utilize methods of nonlinear and chaotic analysis of time series. Two basic components of this analysis are the reconstruction of the experimental time series state space trajectory of the underlying process and the statistical testing of an null hypothesis. The null hypothesis against which the experimental time series are tested is that the observed AE index signal is generated by a linear stochastic signal possibly perturbed by a static nonlinear distortion. As discriminating statistics we use geometrical characteristics of the reconstructed state space (Part I, which is the work of this paper) and dynamical characteristics (Part II, which is the work a separate paper), and "nonlinear" surrogate data, generated by two different techniques which can mimic the original (AE index) signal. The null hypothesis is tested for geometrical characteristics which are the dimension of the reconstructed trajectory and some new geometrical parameters introduced in this work for the efficient discrimination between the nonlinear stochastic surrogate data and the AE index. Finally, the estimated geometric characteristics of the magnetospheric AE index present new evidence about the nonlinear and low dimensional character of the underlying magnetospheric dynamics for the AE index.

1 Introduction

In previous papers about magnetospheric chaos (Pavlos et al., 1992a,b, 1994) we used two different approaches in order to support the hypothesis of low-dimensional magnetospheric chaos. In the first approach we presented a nonlinear analysis of the magnetospheric AE index time series and in the second one we developed an appropriate nonlinear electric circuit model. These studies were the continuation of a series of papers about the possible existence of magnetospheric chaos (Pavlos, 1988; Baker et al., 1990; Vassiliadis et al., 1990; Klimas et al., 1991; Shan et al., 1991; Vassiliadis et al., 1992; Price and Prichard, 1993; Prichard and Price, 1993). However, a series of noticeable studies has given strong evidence against the hypothesis of magnetospheric chaos and indicates the significant role of the externally driven process for the AE index profile (Prichard and Price, 1993; Price et al., 1994; Takalo and Timonen, 1994; Prichard, 1994). For an extended review of studies of the nonlinear dynamics of the magnetosphere see Klimas et al. (1996). Certainly the above criticism showed that the supposition of magnetospheric low-dimensional chaos was not well founded so far.

In a series of papers, which are going to follow, we include new results about magnetospheric dynamics and the hypothesis of low-dimensional chaos. In this first one, we use four distinct geometric parameters derived from the slope of the correlation integral as discriminating statistical procedures in order to test the null hypothesis of stochastic signals, which have the same power spectrum and amplitude distribution as the original data. As we show in detail in this work the use of appropriate characteristics of the reconstructed phase space trajectory indicates significant difference between statistically and nonlinearly transformed stochastic signals and the AE index time series. The AE index describes the magnetospheric dynamics during magnetospheric substorms (see Section 3).

A finite length time series with broadband spectrum, as the AE data, may be a realization of a stochastic process or of a low dimensional deterministic chaotic process (Eckmann and Ruelle, 1985). On the other hand, some geometrical or dynamical characteristics (low correlation dimension or positive Lyapunov exponents) of the low dimensional chaotic dynamics can be observed from particular linear stochastic dynamics. Thus the analysis of experimental time series has to confront the problem of distinguishing between stochastic and deterministic dynamics. A first step in this direction is to detect nonlinear dynamics in the data. In this paper we face this problem for the case of the AE index time series by examining geometrical characteristics of the signal.

In Section 2, we present the background of chaotic anal-

Correspondence to: G. P. Pavlos

ysis including the embedding theory, the surrogate data test and the geometrical quantities used as discriminating statistics. In Section 3, we present the results about the discrimination between the AE index time series and the surrogate data, while the discussion about the results are presented in Section 4.

2 Theoretical framework

2.1 Embedding theory and phase space reconstruction

The earth's magnetosphere is a system of magnetized plasma, which microscopically is an infinite dimensional system, the dynamics of which is mirrored in the ground measured AE index. Some kind of "self-organization" may give rise to system evolution on a low dimensional manifold M of dimension d. This means that the magnetosphere can be described macroscopically by a low dimensional dynamical system of n macroscopic degrees of freedom with $n \geq d$. For linear systems, "self-organization" is more an externally driven process described by the external parameters of the system. For nonlinear and dissipative systems, however, it is possible that the system evolves by its internal dynamics in such a way that the corresponding phase space flow contracts on sets of lower dimensions which are called attractors.

Following the latter assumption, the connection of an experimental time series $x(i) = x(t_i)$ (for discrete time t_i) to the supposed underlying dynamics $\mathbf{s}(t) = \mathbf{f}^t(\mathbf{s}_0)$ is established with the state space reconstruction (Ruelle and Takens, 1971; Takens, 1981), based on Whitney's theorem (Whitney, 1936) that a d-dimensional manifold M can be embedded in R^m if $m \geq 2d+1$, i.e. there exists a smooth $\Phi : \mathbf{M} \to R^m$.

Let $\mathbf{x}(t) = \mathbf{\Phi}(\mathbf{s}(t))$ be the points on the reconstructed trajectory for the embedding $\mathbf{\Phi}$. Then the dynamics on the original attractor is equivalently represented in the mirror dynamical flow $\mathbf{x}(t) = \mathbf{F}^t(\mathbf{x}_0)$ of the reconstructed phase space R^m according to

$$\mathbf{F}^t(\mathbf{x}_0) = \mathbf{\Phi}(\mathbf{s}) \circ \mathbf{f}^t(\mathbf{s}_0) \circ \mathbf{\Phi}^{-1}(\mathbf{x}) \tag{1}$$

Thus, the embedding $\mathbf{\Phi}$ is a diffeomorphism which takes the orbits $\mathbf{f}^t(\mathbf{s}_0)$ in M (for an initial state $\mathbf{s}_0$) to the orbits $\mathbf{F}^t(\mathbf{x}_0)$ in R^m, preserving their orientation and other topological characteristics as eigenvalues, Lyapunov exponents and the dimensions of the attractors, including the correlation dimension (Broomhead and King, 1986; Casdagli et al., 1992).

As it is shown elsewhere the method of reconstructed phase space conserves its significance even when the observed signal is derived by a stochastic process (Argyris et al., 1998; Pavlos et al., 1999).

Assuming the observed signal is $x(i) = h(\mathbf{s}(t_i))$, where h a measurement function, the reconstructed points are, using the method of delays (Packard et al., 1980), $\mathbf{x}(i) = [x(i), x(i+\tau), ..., x(i+(m-1)\tau)]^T$, where τ a delay parameter.

The embedding theory summarized here constitutes the basis of chaotic analysis of experimental time series, allowing for the extraction of information about the dynamics in the original phase space by studying the mirrored dynamics in the reconstructed phase space.

2.2 Geometric Characteristics of experimental time series

2.2.1 Correlation dimension

The theoretical concepts described above permit us to use experimental time series in order to extract useful geometric characteristics, which provide information about the underlying dynamics. Such a characteristic is the correlation dimension D defined as

$$D = \lim_{r \to 0} \frac{d \ln C(r)}{d \ln(r)} \tag{2}$$

where $C(r)$ is the so-called correlation integral for a radius r. When an attracting set exists $C(r)$ reveals a scaling profile

$$C(r) \sim r^d \text{ for } r \to 0 \tag{3}$$

For time series, the correlation integral depends on the embedding dimension m of the reconstructed phase space and reads

$$C(r,m) = \frac{2}{N(N-1)} \sum_{i=1}^{N} \sum_{j=i+1}^{N} \Theta(r - \|\mathbf{x}(i) - \mathbf{x}(j)\|) \tag{4}$$

where $\Theta(a) = 1$ if $a > 0$ and $\Theta(a) = 0$ if $a \leq 1$, and N is the length of the time series. The scaling exponent $d(m)$ increases m and saturates at a final value D for a sufficiently large embedding dimension m_0. Theoretically, this m_0 is the smallest integer larger than D according to Ding et al. (1993), but in practice m_0 may attain larger values depending also on τ (Kugiumtzis, 1996). Note that an embedding may require a larger m.

For periodic attractors the correlation dimension D becomes equal to the topological dimension d of the manifold M, which includes the attractor. Usually for a strange attractor, D obtains a fractal value.

When the slopes $d(m)$ of the correlation integrals reveal a plateau at low values of r and the plateau converges for increasing m, then this is strong evidence for low-dimensionalit of the underlying dynamics to the observed signal. The stocha tic component behaving as noise in the experimental time series, destroy the plateau and saturation profile at low values of the radius r and makes the derivation of reliable dimension estimates difficult.

2.2.2 False neighbors and embedding dimension

Besides the correlation dimension the method of false nearest neighbors can also give an estimation of the smallest sufficient embedding dimension m_0. When the trajectory of the system is reconstructed in a space of low dimensionality, then it is possible to have self- crossings and that gives rise to false neighbor state vectors. This is gradually improved as the embedding dimension is increased and for a large enough embedding dimension m_0 false crossings and false neighbors

disappear. Let $\mathbf{x}(j)$ be the nearest point to $\mathbf{x}(i)$ for an embedding dimension m. Then their distance is given by

$$r_m^2(i,j) = (x(i)-x(j))^2+\cdots +(x(i+(m-1)\tau)-x(j+(m-1)\tau))^2 \quad (5)$$

Passing from m to $m+1$ embedding dimension this distance takes the form

$$r_{m+1}^2(i,j) = r_m^2(i,j)+(x(i+m\tau)-x(j+m\tau))^2 \quad (6)$$

Then if

$$\frac{|\mathbf{x}(i+m\tau)-\mathbf{x}(j+m\tau)|}{r_m} > R_T \quad (7)$$

the nearest neighbors at time i are declared as false (Abarbanel et al., 1993). The threshold value R_T is estimated to be in the range $10 \leq R_T \leq 50$. According to this criterion as the embedding dimension m increases to a characteristic value m_0 the percent of false nearest neighbors may drop to zero. If this is actually observed for a time series, it consists of a positive sign for the existence of low-dimensional dynamics underlying the observed signal.

2.3 The method of surrogate data

According to Eq. (3) the scaling properties of the correlation integral as $r \to 0$ and the saturation of the scaling exponent $d(m) \to D$ as m increases are necessary conditions for the existence of low-dimensional dynamics underlying to the experimental time series. However, it has been shown that these conditions are not efficient in order to conclude low-dimensional dynamics from an experimental time series with broadband power spectrum, as they can be reached also by stochastic systems (Osborne and Provenzale, 1989; Provenzale et al., 1991). Moreover, according to Theiler (1991), the concept of low correlation dimension (fractal or integer) can be applied to time series in two distinct ways. The first one indicates the number of degrees of freedom in the underlying dynamics and the second quantifies the self-affinity or "crinkliness" of the trajectory through the phase space. In the first case, the scaling and saturation profile are caused by the recurrent character of the reconstructed trajectory, i.e. by uncorrelated in "time" and correlated in "space" state points. In the second case, they are caused by time correlated state points that are uncorrelated in space. In order to discriminate between the two cases, known as dynamic and geometric low-dimensionality, we restrict the sum in Eq. (4) to pairs $(\mathbf{x}(i), \mathbf{x}(j))$ with $|i-j| > w$, for the Theiler parameter w larger than the decorrelation time of the time series.

When low-dimensionality is persistent as a dynamic characteristic after the application of Theiler's criterion, then we have to decide first between linearity and nonlinearity and then between chaoticity and pure stochasticity. By the term chaoticity we mean the case that the deterministic component of the process is prevalent and reveals low-dimensional chaos. For a stochastic process, the deterministic component may correspond to low dimensional and even nonlinear and chaotic dynamics, but its effect can be hardly observed as the process is driven mainly by noise. Therefore, we focus here on the solution of the first problem, i.e. determining whether the AE index time series is linear or nonlinear. This is done by following the method of "surrogate" data (Theiler et al., 1992b,a).

The method of "surrogate" data includes the generation of an ensemble of data sets which are consistent to a null hypothesis. According to (Theiler et al., 1992b), the first type of null hypothesis is the linearly correlated noise which mimics the original time series in terms of autocorrelation function, variance and mean. The second and more general null hypothesis takes into account that the observed time series may be a nonlinear monotonic static distortion of a stochastic signal.

Every Gaussian process is linear while a non-Gaussian process can be linear or nonlinear. An experimental time series may show nonlinearity in terms of a non-Gaussian point distribution, which may be due to a nonlinear measurements function of linear underlying dynamics. In this case, the generated "nonlinear" surrogate data mimic the original time series $x(i)$ in terms of autocorrelation function and probability density function $p(x)$. It is always possible for a nonperiodic time series of finite length to be a particular realization of a noise process or of a low-dimensional deterministic process. Therefore, it is a statistical problem to distinguish a nonlinear deterministic process from a linear stochastic process. For this purpose we use as discriminating statistic a quantity Q derived by a method sensitive to nonlinearity, as the correlation dimension estimation. The discriminating statistic Q is calculated for the original and the surrogate data and the null hypothesis is verified or rejected according to the value of "sigmas" S

$$S = \frac{\mu_{obs}-\mu_{sur}}{\sigma_{sur}} \quad (8)$$

where μ_{sur} and σ_{sur} is the mean and the standard deviation of Q on the surrogate data and obs is the mean of Q on the original data. For a single time series, μ_{obs} is the single Q value (Theiler et al., 1992b).

The significance of the statistics is a dimensionless quantity, but we follow here the common parlance and we report it in terms of the units of S "sigmas". When S takes values higher than 2-3 then the probability that the observed time series does not belong to the same family with its surrogate data is higher than 0.95-0.99, correspondingly.

For testing the second more general null hypothesis described above we follow the algorithm of Theiler (Theiler et al., 1992b), as well as the algorithm of Schreiber and Schmi (Schreiber and Schmitz, 1996). Both algorithms create stocha tic signals which have the same autocorrelation and amplitude distribution as the original time series.

According to the first algorithm, first a white Gaussian noise is reordered to match the rank of the original time series (this is to make the original time series Gaussian). Then the

phases of this signal are randomized (to destroy any possible nonlinear structure). Finally, the original signal is reordered to match the rank of the above constructed coloured noise (to regain the original amplitude distribution). The derived shuffled time series is the surrogate time series.

The algorithm of Theiler was improved by Schreiber and Schmitz by a simple iteration scheme in order to strengthen the ability of the surrogate data to fit more exactly the autocorrelation and power spectrum of the original time series. Starting with a white noise signal, its Fourier amplitudes are replaced by the corresponding amplitudes of the original data. The rank order of the derived stochastic signal is used to reorder the original time series. By this reordering, the matching of amplitude distribution is succeeded, but the matching of power spectrum achieved in the first step is altered. Therefore, the two step process is repeated several times until the change in the matching of power spectrum is sufficiently small.

2.4 Critical Parameters for the statistical comparison between the AE index time series and the surrogate data

In order to be able to utilize as much as we can from the application of the method of the surrogate data, we must decide on the appropriate geometric parameters of the reconstructed trajectory which are going to be used as discriminating statistics. For this purpose we use the following quantities:

a The slopes of the correlation integral

b The standard deviation (S_{dev}) of the slopes

c The length of the scaling (L_{scal})

d The cumulative distances of the slopes (F_{dis})

e The percent of false nearest neighbors (f_{ngb})

We present now some theoretical explanations for the use of the above magnitudes. The standard deviation S_{dev} of the slopes is a function of $\ln(r)$ (r is the distance radius in the reconstructed phase space), defined as

$$S_{dev}(\ln r_k) = \sqrt{\frac{\sum_{i=1}^{N}(D(\ln(r_{kl})) - \bar{D}(\ln(r_k)))^2}{N}} \qquad (9)$$

where $\{\ln(r_k), k = 1, 2 \cdots n\}$ is a fine partition of a predefined interval $\Delta \ln(r) = [\ln(r_a), \ln(r_b)]$ of possible scaling (r_a not too small, r_b not too large), and $D(\ln(r_{kl})), l = 1, \cdots N$, are the estimated values of the slopes at every point r_{kl} in the subinterval $[\ln(r_k), \ln(r_{k+1})]$ of the above partition. By $\bar{D}(\ln(r_k))$ we denote the mean value in the interval $(\ln(r_k), \ln(r_{k+1}))$. It is important to note that in the region where there is scaling of the correlation integral, the values of the function $S_{dev}(ln(r))$ must be close to zero.

The magnitute of the length of scaling is defined by the relation

$$L_{scal} = \ln(r_2) - \ln(r_1) \qquad (10)$$

where $[r_1, r_2]$ is the interval of distance r in which the standard deviation of the slopes S_{dev} is smaller than a quantity ϵ whose value is close to zero. A sufficiently large L_{scal} is a necessary condition for a dynamics evolving on an attractor. So, an estimation of the correlation dimension is without physical meaning when L_{scal} is not large enough and the local standard deviation of the slopes S_{dev} tends to zero.

However, when we compare the surrogate data with the original time series then it is possible that the scaling profile to be observed for both data types, but the saturation value for the slopes to be different for the original time series and for its surrogate data. Therefore, we introduce a new geometrical parameter, the cumulative distance F_{dis}, which is appropriate for the aforementioned comparison, defined by the equation

$$F_{ds}(D_1, D_2) = \sqrt{\frac{\sum_{i=1}^{N}(D_1(\ln(r_i)) - D_2(\ln(r_i)))^2}{N}} \qquad (11)$$

where $\{\ln(r_i), i = 1, 2, ..., N\}$ is a finite partition of the interval $[ln(r_1), ln(r_2)]$ along which the slope reveals plateau profile. In our case D_1 corresponds to the slope segment for the signal and D_2 is a given plateau, thus $D_2 \equiv constant$.

The last quantity, i.e. the percent of false nearest neighbors f_{ngb}, has been already presented in subsection 2.2.

3 Data analysis and results

The AE index describes the Auroral-zone magnetic activity which is related with the global magnetospheric dynamics through a complex system of currents. The magnetospheric dynamics during substorms is manifested as strong variability of the magnetospheric and ionospheric electric currents especially the auroral electrojets (McPherron, 1995). Disturbances in the Earth's magnetic field produced by currents in the magnetosphere and ionosphere are commonly described by a number of magnetic activity indices, which are derived from certain physical parameters connected to the dominant phenomena causing the disturbance. The indices AU, AL, and AE give a measure of the strength of the auroral electrojets and are defined with the use of traces of the horizontal component (H) of the geomagnetic field measured by a world-wide chain of auroral-zone magnetic observatories (Davis and Sugiura, 1966). AU is the maximum positive disturbance (upper envelope) recorded by any station in the chain. AL is the minimum disturbance defined by the lower envelope of the traces of the chain. AE is defined by the separation of the envelopes (AE = AU-AL) in order to obtain a better measure of the strength of the auroral electrojets.

Figure 1a shows measurements of AE index which correspond to the second half of the year 1978. The sampling rate of the original signal was one minute while the time series used in this paper contains $N_T = 32768$ data points that are the eight minute averages of the entire time series, rounded to the nearest power of two. That is the original time series contains $N \cong 250.000$ data points. This time series has much longer length than the time series used in our previous work (Pavlos et al., 1992b, 1994) as well as in the works of other

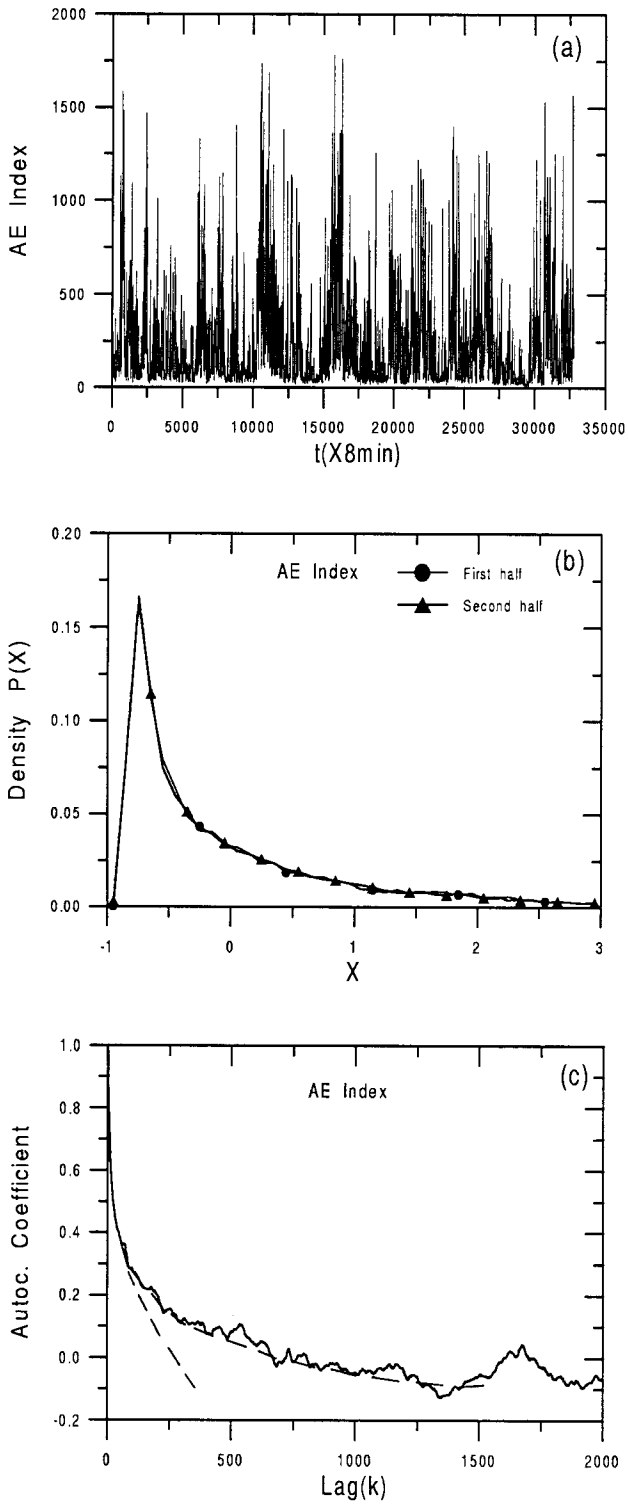

Fig. 1. (a) AE index measurements with eight minute time resolution corresponding to the second half of the year 1978. The bursting character of the AE index is obvious and indicates the strong coupling of the magnetosphere with the solar wind. (b) Amplitude distribution for the first and second half of the AE index time series. It is apparent the stationarity of AE index. (c) The autocorrelation coefficient for the first 2000 units of lag time indicates two different processes. The first corresponds to an abrupt decay of the autocorrelation coefficient and the second to a slow decay.

scientists. The stationarity of the time series is tested by estimating the amplitude distribution for the first half of the data set and for the second half of it (see Fig. 1b). The amplitude distributions are the normalized ones as we subtract the mean and we have divided by the standard deviation. From the same figure it is obvious that the AE index time series reveals non-Gaussian amplitude distribution.

The random character of the AE time series is revealed by the decaying shape of the autocorrelation function (Fig. 1c) showing an abrupt decay during the first 100-200 minutes and a slow long decay afterwards. This profile of the autocorrelation function could possibly be caused by two different mechanisms. A dynamical one which corresponds to the abrupt decay and a stochastic one (coloured noise) which is responsible for the slow decay. The two discontinuous lines in Fig. 1c reveal the two different mechanisms. Of course the abrupt decay can not be explained solely as a chaotic behaviour as it is possible to be caused by a static nonlinear distortion of a linear stochastic system.

3.1 Geometric characteristics of AE index time series

In the following, we present the results of the analysis of the AE index in two stages. First, we show the geometric characteristics of AE index data and then we compare them with the corresponding characteristics of the "nonlinear" surrogate data.

Figure 2a shows the slopes D of the correlation integral for embedding dimension $m = 20$ and delay times $\tau = 10-100$. It is obvious that there is a scaling of the correlation integral $(C(r,m) \sim r^{d(m)})$ for $\tau = 30-60$ and for low values of the distance r in the reconstructed phase space. In this estimation Theiler's parameter takes the value $w = 100$. The scaling region is located for $\ln(r)$ between 5-6.5, while for $\tau = 60$ we have the best scaling. Figure 2b shows the slope $D(ln(r))$ for $m = 20, \tau = 60$ and w between 0-500. In this case, we can observe that for $w > 5$ the slope remains invariant with an apparent plateau in a long region $\Delta ln(r) \cong 5-6.5$, of the distance r. For values of $ln(r) < 5$ there is scaling only for $w = 0$ caused by time correlated state points, while for values of $ln(r) > 5$ the scaling is caused by time uncorrelated states due to space recurrence and space correlation. This means that the AE index data are possibly connected with low-dimensional dynamics which creates a recurrent trajectory in phase space. Figure 2c shows the slopes for embedding dimension $m = 8-20, \tau = 60$ and $w = 100$. Figure 2d presents the mean values of the scaling exponents $d(m)$ estimated at the scaling region. The dashed lines in Figs. 2c-d indicate the tendency for low value saturation of the slopes and scaling exponents at the level $D \cong 4-6$, for a long range of $m = 8-20$. However, as the signal of the AE index may include a stochastic component the low value saturation profile can be expected only in approximation. Taking into account that the degrees of freedom d of the underlying dynamics is in the region $D + 1 \leq d \leq 2D + 1$, the above result is in agreement with the dimension used in theoretical models for the magnetospheric dynamics (Baker et al., 1990;

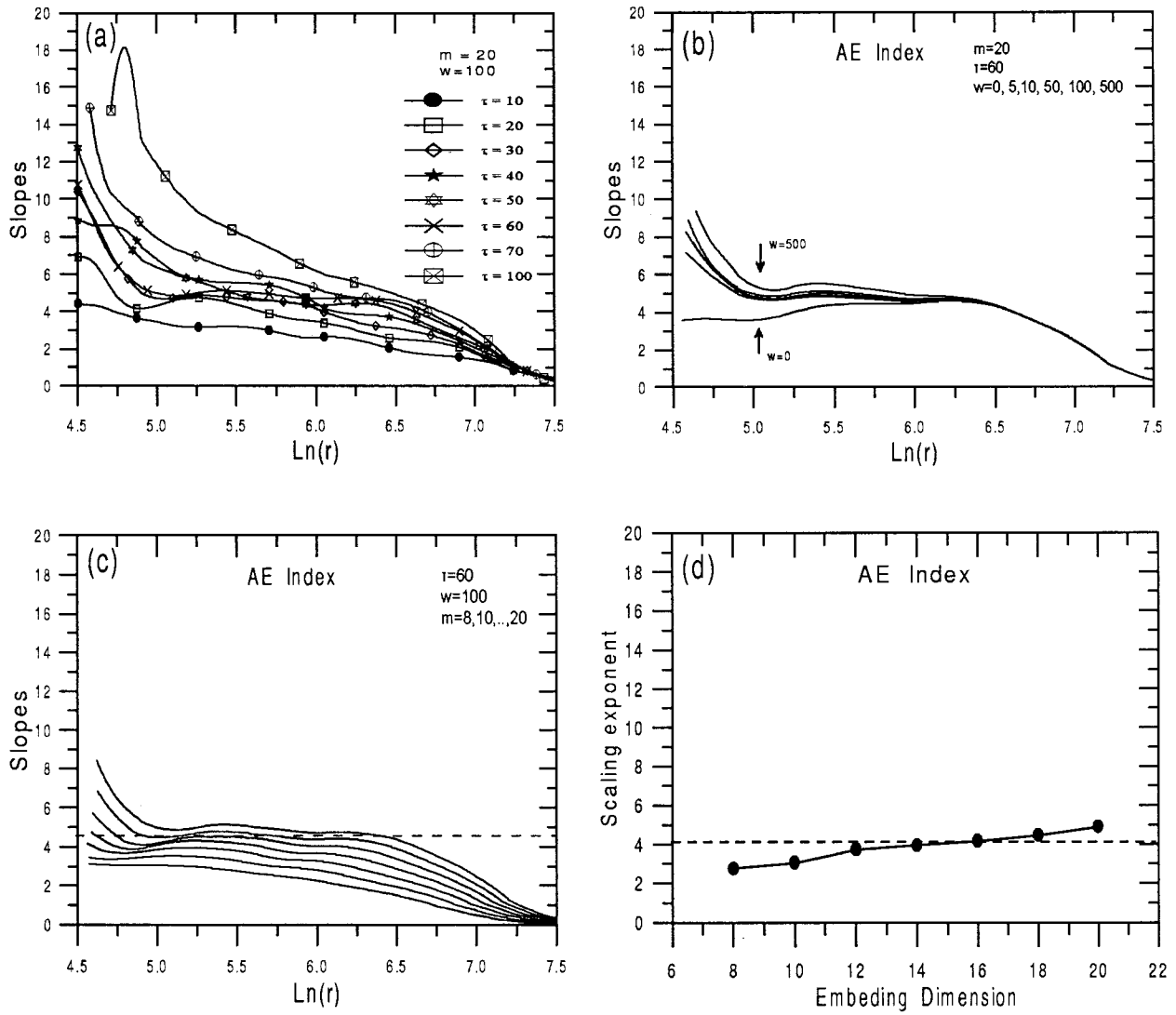

Fig. 2. (a) The slopes of the correlation integral as a function of the radius r estimated for embedding dimension $m = 20$, delay time $\tau = 10 - 100$ units of sampling time and the Theiler parameter $w = 100$. For delay time $\tau = 30 - 60$ we observe the best scaling. (b) The same with (a) for delay $\tau = 60$ and $w = 0 - 500$, showing that there is no significant change of the slopes for $w = 5 - 500$. (c) The same with (a) for $\tau = 60, w = 100$ and embedding dimension $m = 8 - 20$. (d) The scaling exponent $d(m)$ as a function of the embedding dimension m estimated along the scaling region. For all m, the scaling exponent takes values lower than 6 while there is a tendency for saturation in the range of values $D \cong 4 - 5$.

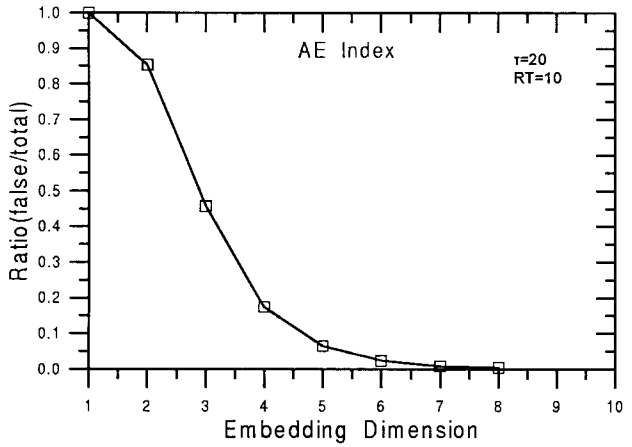

Fig. 3. The ratio of the false to the total nearest neighbors as a function of the embedding dimension $m(\tau = 20)$. The ratio converges to zero for embedding $m \geq 8$.

Klimas et al., 1991; Pavlos et al., 1994).

Figure 3 shows the ratio of false to total nearest neighbors as a function of the embedding dimension m estimated for delay time $\tau = 20$ and threshold value $R_T = 10$. The figure shows that the ratio of false nearest neighbors drops to zero for embedding dimension $m \cong 7 - 8$. This result implies that the embedding of the attractor in an 8-dimensional phase space is enough for the false crossings and false neighbors to disappear. This is in accordance with the previous result about the dimensionality of the underlying magnetospheric dynamics as it was concluded by the estimate of the correlation dimension.

3.2 Statistical test of the null hypothesis

The non-Gaussian amplitude distribution of the AE index can possibly imply the nonlinearity of the signal under appropriate conditions. However, the nonlinearity of a signal can be static or dynamic. As discussed in subsection 2.3 a random like and non-Gaussian signal can be possibly caused by a deterministic nonlinear and even chaotic underlying process or by a stochastic process observed through a nonlinear static distortion. Figure 4 presents three surrogate signals and the corresponding slopes of the correlation integrals for different embedding dimensions. The two first surrogate signals were generated by using the algorithm of (Theiler et al., 1992b,a) and are symbolized as T-surrogates. The third one was generated by using the algorithm of Schreiber and Schmitz (1996) and is symbolized as S-surrogate. Both types of surrogates are supposed to preserve the amplitude distribution and the power spectrum (and thus the autocorrelation as well) of the AE signal. Thus both surrogate types are representative for a static nonlinear distortion of a stochastic infinite dimensional linear process. The general profile of the surrogate signals (shown in Figs. 4a, c, e) is similar to the original AE index time series (shown in Fig. 1a). The profile of the slopes may be similar to that for the original signal as we can conclude by comparing Fig. 4b and Fig. 2c or to be significantly different as Fig.4d and Fig. 2c show. An intermediate state is that shown in Fig. 4f which in some way approaches the profile of Fig. 2c, without being completely similar. The existence of at least one stochastic signal which can reveal significant similarity in terms of slopes with the AE index signal indicates that the AE index may belong to the family of linear stochastic signals considered here. To test this null hypothesis we generated two groups of forty statistically independent T-surrogate and S-surrogate signals, respectively.

Fig. 5a shows the autocorrelation coefficient for the 40 T-surrogate and for the original signal. Fig. 5b shows the same for the S-surrogate data. The autocorrelation coefficients for the S-surrogate data are concentrated close to that of the original. The closeness is actually determined by the convergence limit of the algorithm. For the T-surrogate data the autocorrelation coefficients are scattered and show a tendency towards a positive bias at least for small lags (see Fig. 5c).

In the following, we present results of the statistical test of the null hypothesis by using the five geometrical quantities described in subsection 2.4 as discriminating statistics.

3.2.1 Slopes of the correlation integrals

Fig. 6a includes the slope of the correlation integral estimated in a 20-dimensional state space for the AE index and its T-surrogate data. Fig. 6b corresponds to Fig.6a and shows the mean value and standard deviation of the slopes for the T-surrogate data, and the slope of the AE index. Only for very few T-surrogate signals the slope approaches that of the original signal, particularly for small distances as shown in Fig. 6a. This is better manifested in Fig.6c where it can be observed that the significance is larger for small r. However, a clear discrimination between the AE index and its surrogate signals can not be established as the significance does not exceed the level of 2 sigmas for any but very small r-values. As shown in Fig. 6c, $S \geq 2$ is attained only for $ln(r) \cong 5$, and then we can reject the null hypothesis with 95% confidence.

Figures 7a-c are similar with Figs. 6a-c but correspond to the second group of the S-surrogate data. Here the discrimination is more clear as the significance of the statistics stays within the region $\sim 2 - 3$ sigmas for a large interval of small r-values. In this case we can reject the null hypothesis with confidence $> 95\%$. However, the direct comparison of the local slopes alone is not sufficient for the decision about the null hypothesis because it does not contain information about the scaling character. As shown in Fig. 6a and Fig. 7a the slopes of the surrogate signals generally do not reveal significant scaling profile. For this reason in the following we study the geometrical quantities appropriate for the comparison of the scaling character between AE index and its surrogate data, as they were introduced in subsection 2.4.

3.2.2 Standard deviation S_{dev} of the slopes

The standard deviation of the slopes S_{dev} is estimated for the AE index and its T-surrogate data in a 20-dimensional

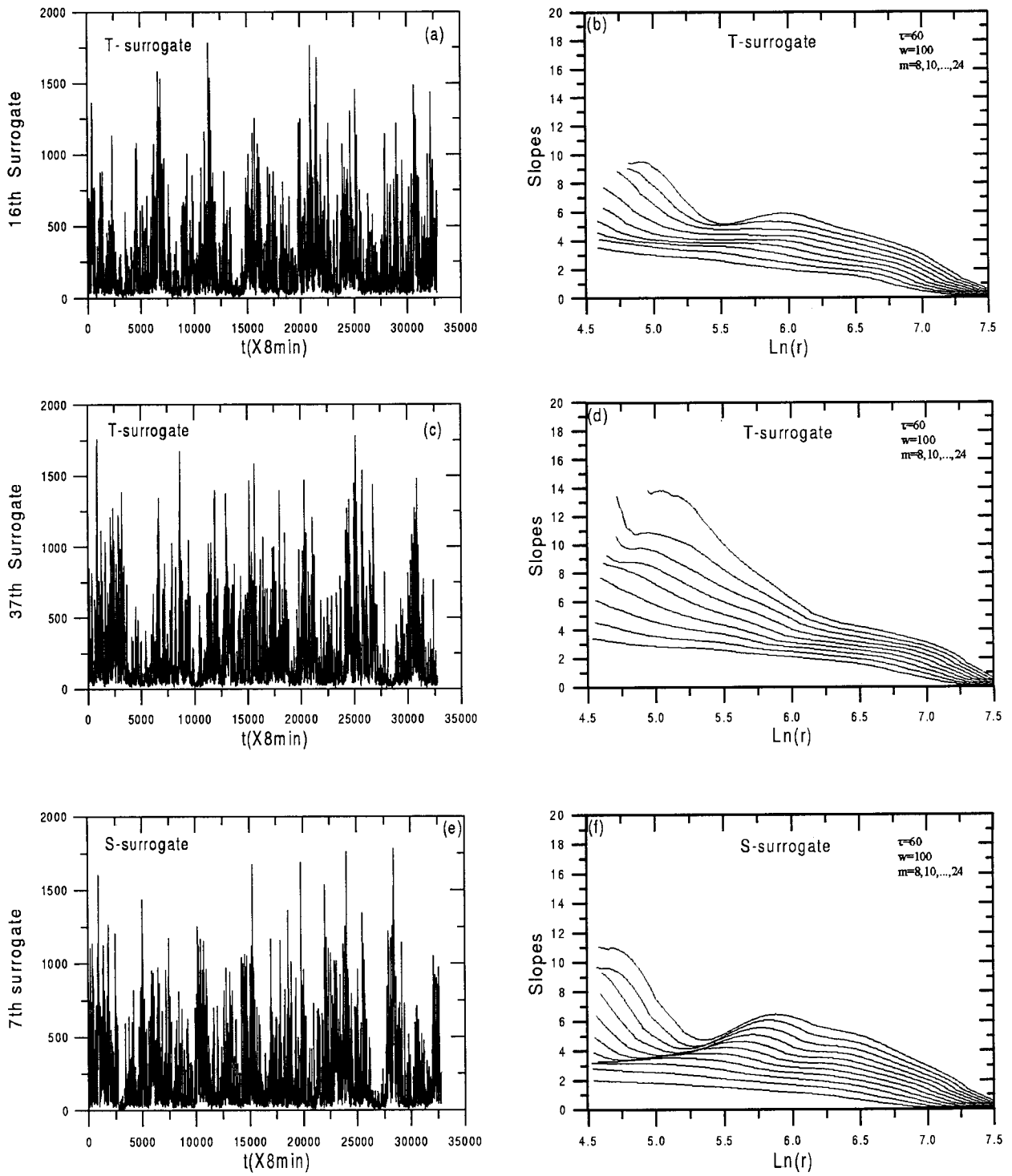

Fig. 4. (a) The T-surrogate data which mimics the amplitude distribution and the power spectrum of the AE index. (b) The slopes of the correlation integrals for the T-surrogate time series of Fig. 4a. It is obvious the similarity with Fig. 1a and Fig. 2c. (c,d) Similar with (a,b) but for a T-surrogate signal. Here the slopes are different than ones of the original signal. (e,f) Similar with (a,b) but for S-surrogate data.

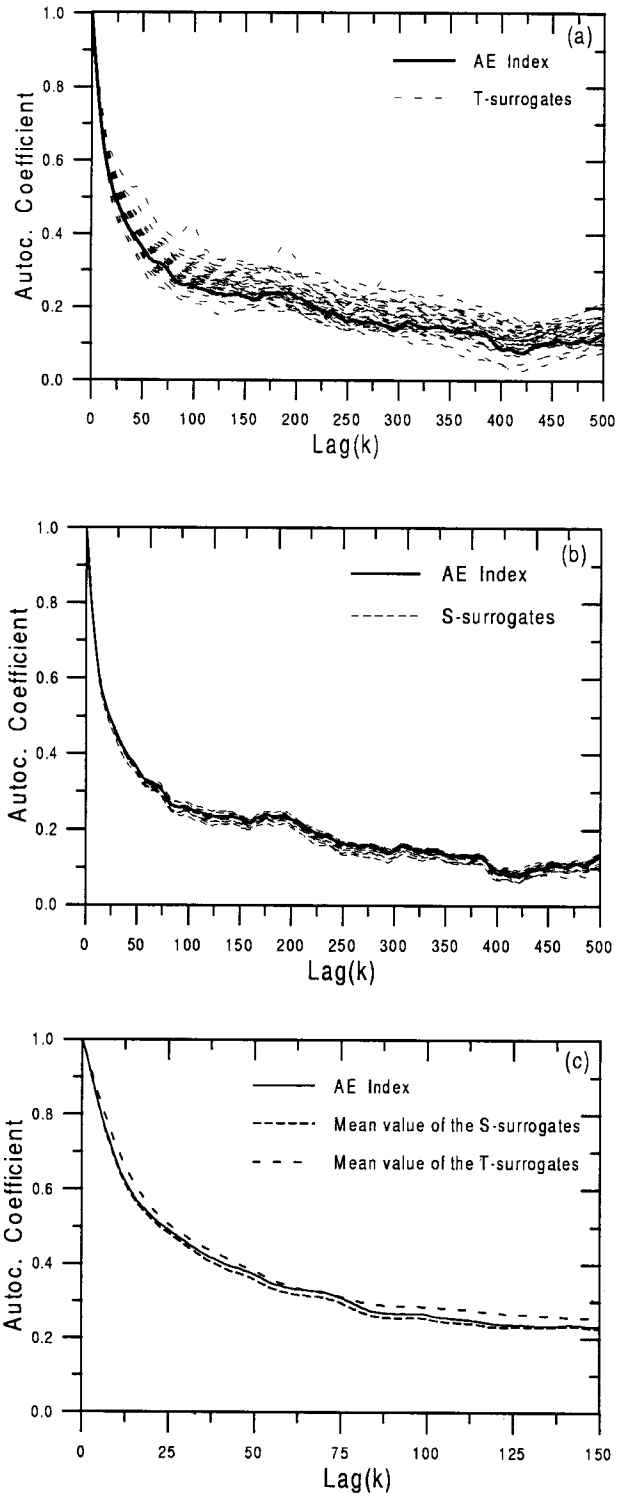

Fig. 5. (a) The autocorrelation function estimated for the group of 40 T-surrogate signals. (b) The same with (a) but for the group of 40 S-surrogate data. (c) The autocorrelation coefficient of the AE index and the mean value of the autocorrelation coefficients shown in (a) and (b) respectively.

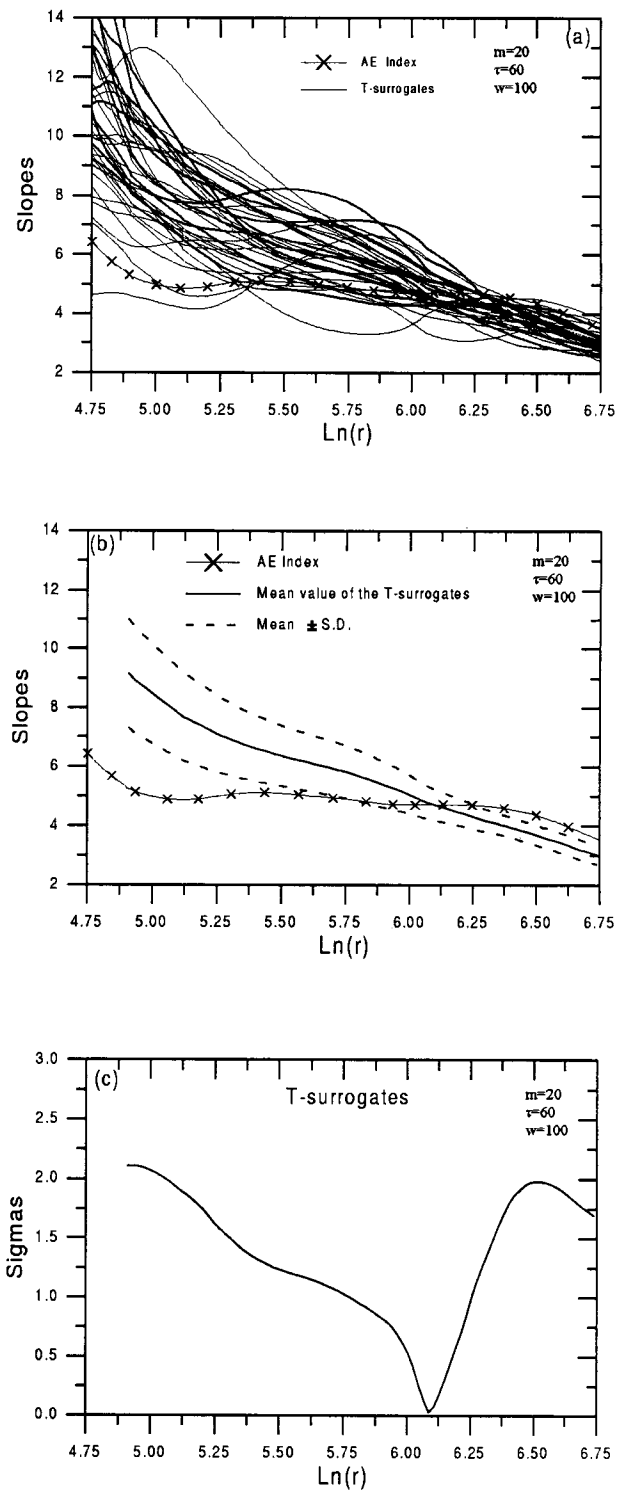

Fig. 6. (a) Slopes of the correlation integrals estimated as function of $\ln(r)$ for the group of 40 T-surrogate data. The parameters of this estimation were $m = 20, \tau = 60$ and $w = 100$. (b) Mean value and mean value $\pm$ standard deviation (S.D.) of the slopes shown in Fig. 6a. (c) The significance for the statistics shown in Figs. 6a-b as a function of $\ln(r)$.

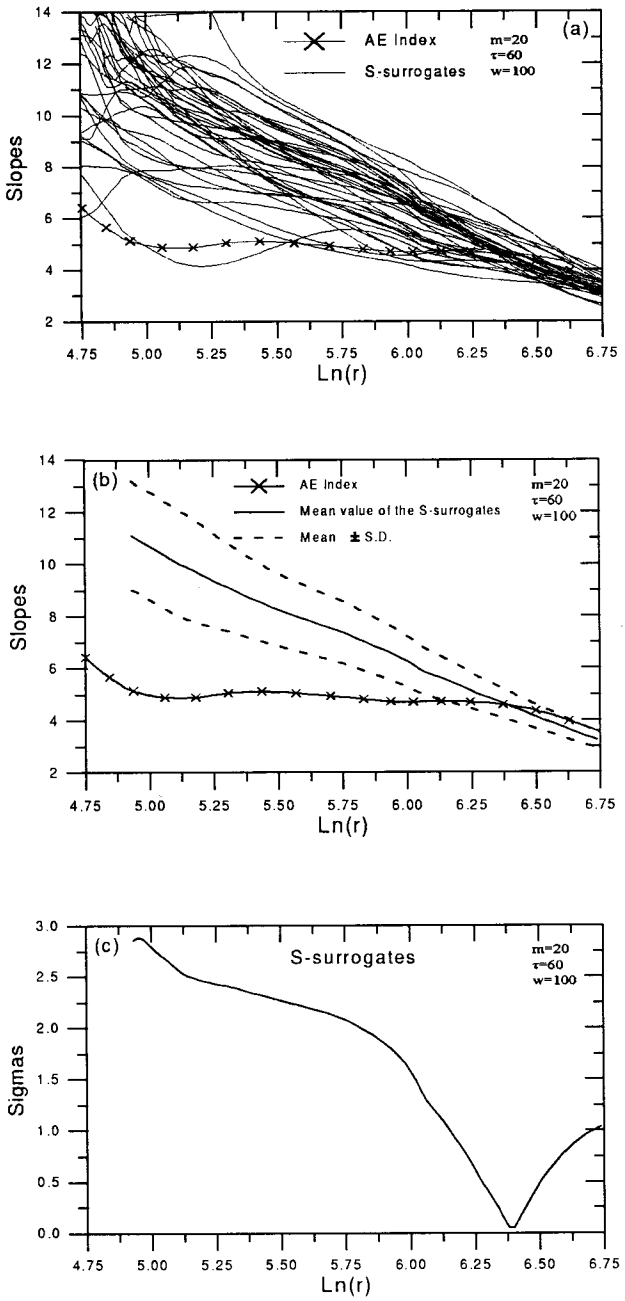

Fig. 7. The same with Fig. 6 but for the S-surrogate data.

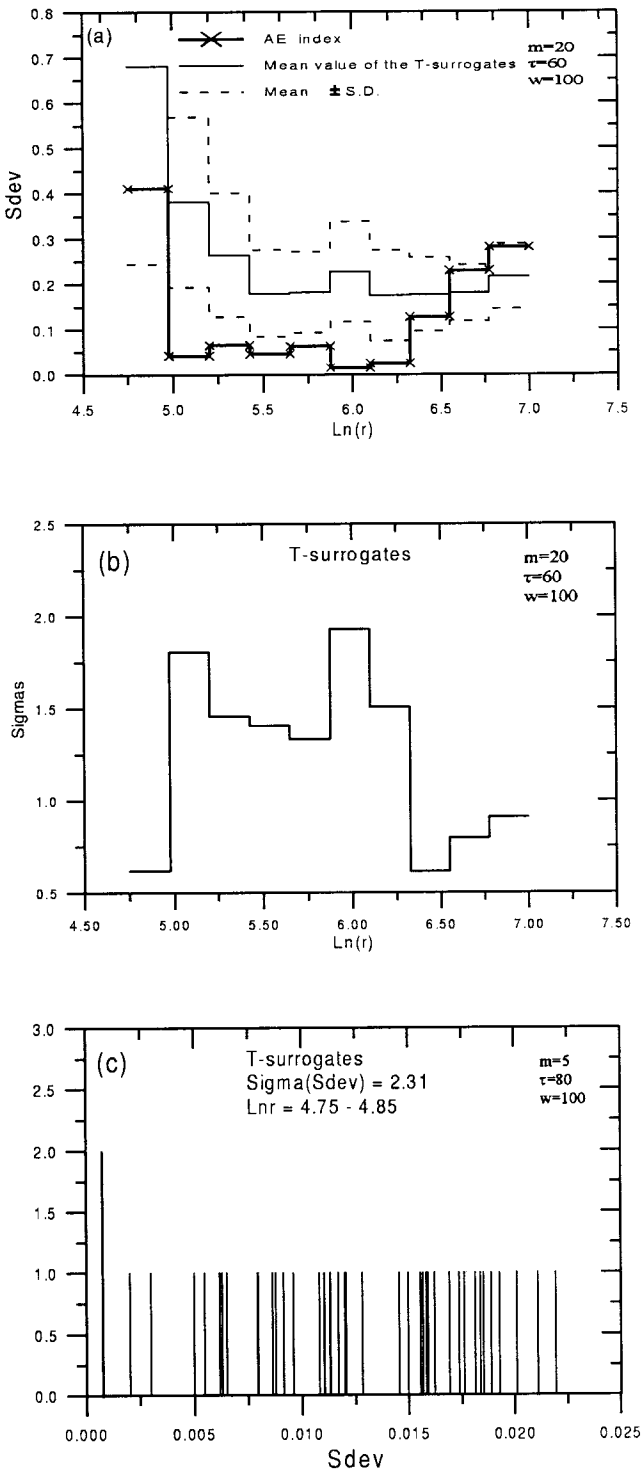

Fig. 8. (a) The mean value and mean value ± standard deviation (S.D.) of the local standard deviation S_{dev} of the slopes for the 40 T-surrogate data shown in Fig. 6a. The local standard deviation S_{dev} for the AE index is also shown. (b) The significance of the S_{dev} as a function of $\ln(r)$. (c) The discriminating statistic S_{dev} for the AE index (shown as the tall line) together with S_{dev} for the 40 T-surrogate data (short lines). For this estimation we have used the embedding parameters $m = 5, \tau = 80, w = 100$, where the maximum value of significance was observed.

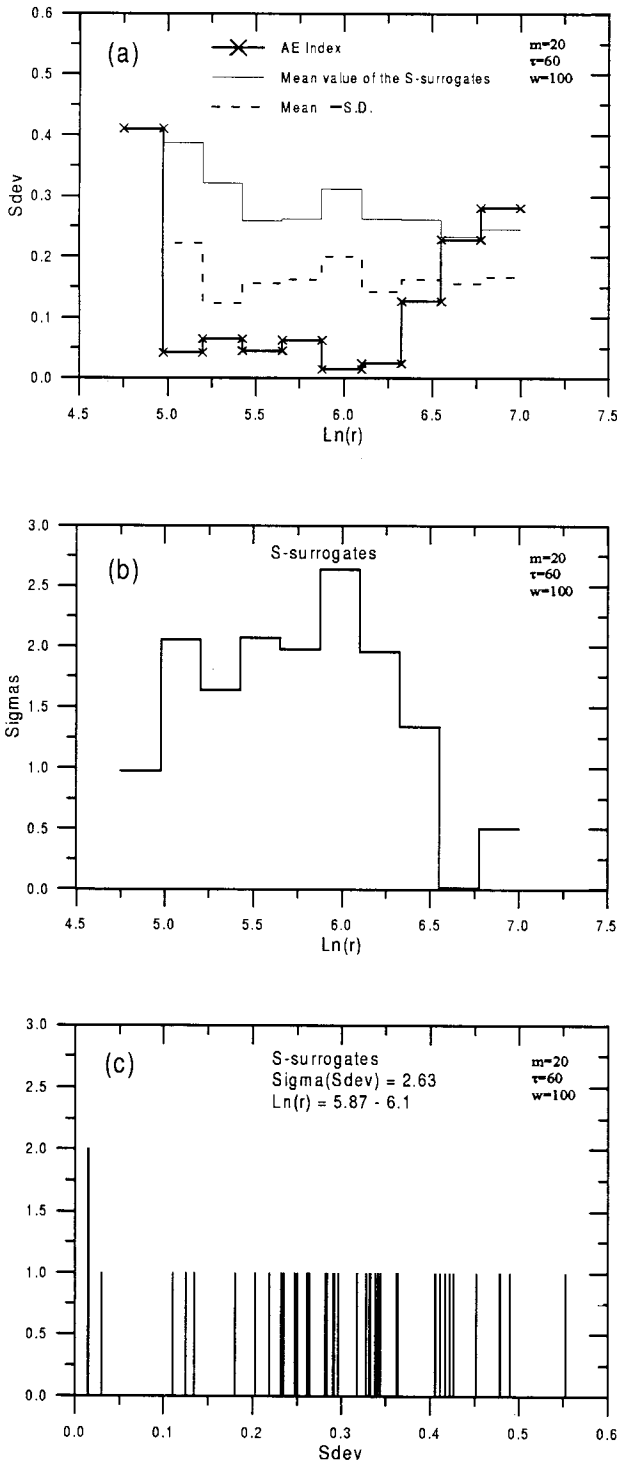

Fig. 9. The same with Fig. 8 but for the S-surrogate data.

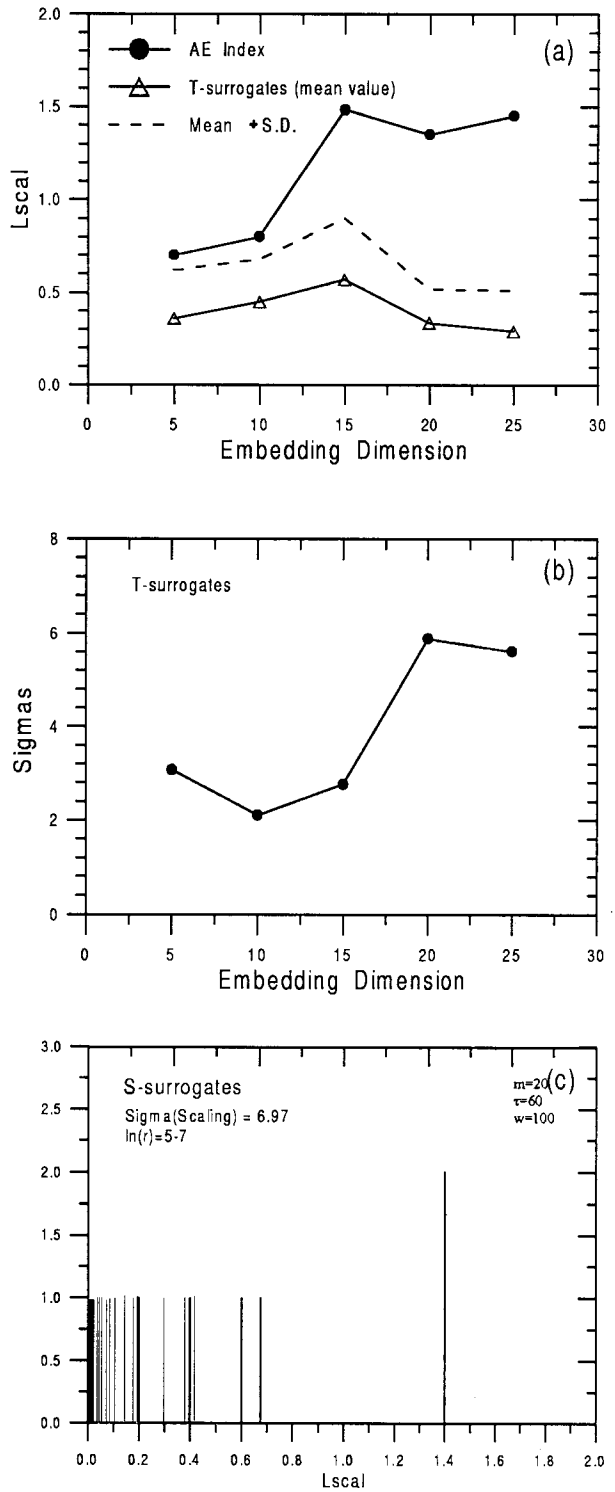

Fig. 10. (a) The mean value and standard deviation of the length of scaling L_{scal} as a function of m estimated for 40 T-surrogate data. The delays $\tau = 80, 55, 60, 60, 60$ were used with $m = 5, 10, 15, 20, 25$ respectively. The L_{scal} for the AE index is shown as well. (b) Significance of the statistic L_{scal} for the T-surrogate data as a function of m. (c) The L_{scal} for the AE index (tall line) and the S-surrogate data (short lines) for a single estimation ($m = 20, \tau = 60, w = 100$). The significance was found to be $S = 6.97$ sigmas.

reconstructed state space, as shown in Fig. 8. For the surrogate data, we present the mean value of S_{dev} and the deviation from the mean. For this estimation we divided the region $\Delta \ln r = 4.75 - 7.00$ in 10 non over-lapping subintervals and computed S_{dev} in each subinterval. By definition, S_{dev} approaches zero when there exists scaling of the correlation integral. In Fig. 8a, we observe that the S_{dev} for the AE signal fluctuates at low values ($S_{dev} \cong 0.05$) in the interval $[5, 6.25]$ of $\ln(r)$ while the corresponding values of S_{dev} estimated for the T-surrogate data are sensibly higher, ($S_{dev} = 0.2 - 0.4$). For this interval of $\ln(r)$ the significance of S_{dev} is in the range of 1.5-2.0 sigmas as shown in Fig. 8b. These values suggest that the rejection of the null hypothesis occurs with confidence $65 - 95\%$, (as the value of 1.5 sigmas corresponds to the probability value 0.65). Figure 8c shows the discriminating statistic of S_{dev} for the AE index (tall line) and the T-surrogate data (short lines) corresponding to the 5-dimensional embedding using $\tau = 80$, which for S_{dev} gives the best discrimination. This figure shows that the difference is clearly significant permitting the rejection of the null hypothesis at a confidence level larger than 95%.

Figure 9 is similar with Fig. 8 but for the S-surrogate data. The S_{dev} for the AE index, is well below the S_{dev} for the S-surrogate data (see Fig. 9a). As shown in Fig. 9b the significance is larger than that of the T-surrogates permitting a more clear discrimination between the original and the surrogate data. That is, for all but one subintervals in the interval $[5, 6.25]$ of $\ln(r)$, the rejection occurs with confidence larger than 95%. The best results obtained are shown in detail in Fig. 9c.

3.2.3 The length of scaling L_{scal}

The length of scaling L_{scal} as defined in section 2.4 is estimated by the maximum length of an interval of $\ln(r)$ for which the standard deviation of the slope of the correlation integral S_{dev} is less than a given value ϵ close to zero, here set to 0.05 according to the previous results. A large L_{scal} supports a physical interpretation of the results on the geometrical characteristics of the reconstructed trajectory. Figure 10a shows the estimated values of L_{scal} for the AE index and the mean value and standard deviation of L_{scal} for the T-surrogate data, as functions of the embedding dimension m. For each m the delay τ giving the best scaling profile for the AE index was used. It is clear that the L_{scal} for the AE index obtains significantly higher values than those for the T-surrogate data. The significance of the discriminating statistic, shown in Fig. 10b, varies in the range of 2-6 sigmas. Figure 10c shows the discriminating statistics of L_{scal} for the S-surrogate data and for a single estimation with $m = 20$. Again the S-surrogate data allow for better discrimination. However, the results on L_{scal} in both cases suggest the rejection of the null hypothesis with confidence $> 95\%$.

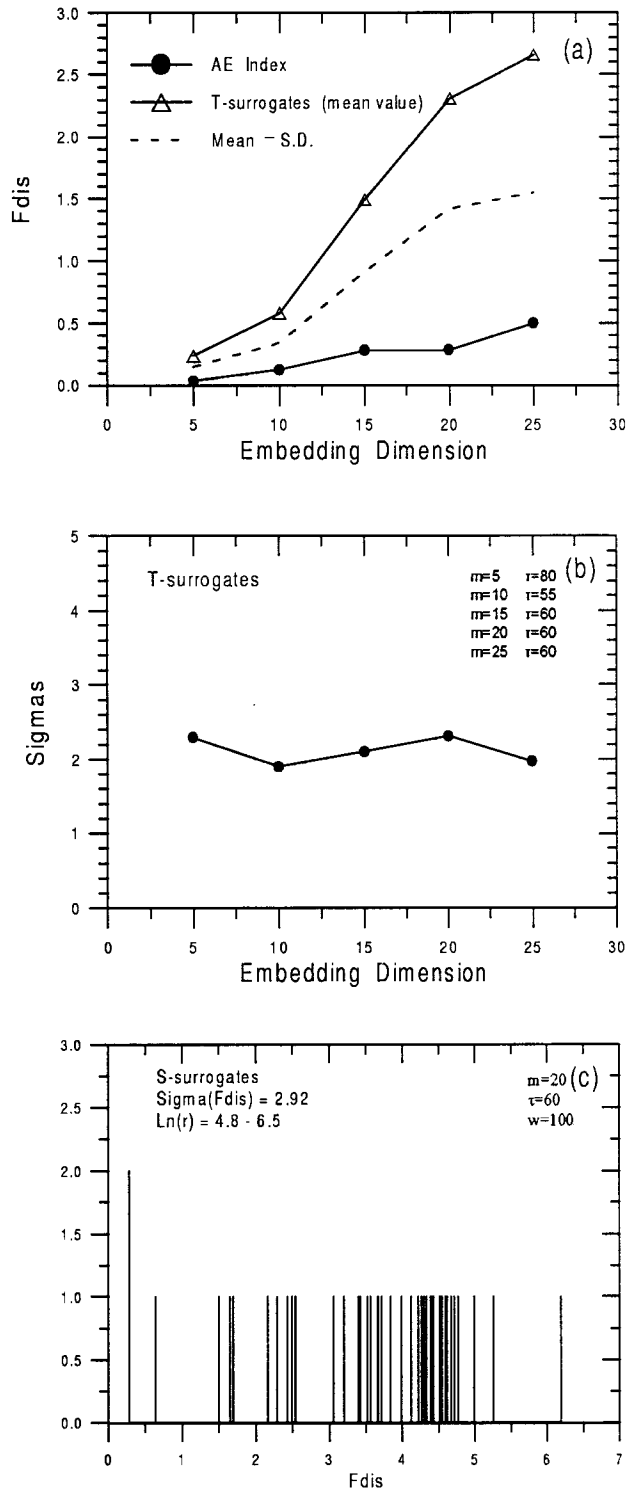

Fig. 11. The same with Fig. 10, but for the parameter of cumulative distance F_{dist}. The estimate of F_{dist} is computed by the deviation of the slope from the plateau of the mean value of the slope of AE index in the interval of $\ln(r)$, for which the scaling profile was observed. This plateau is different for each embedding dimension m.

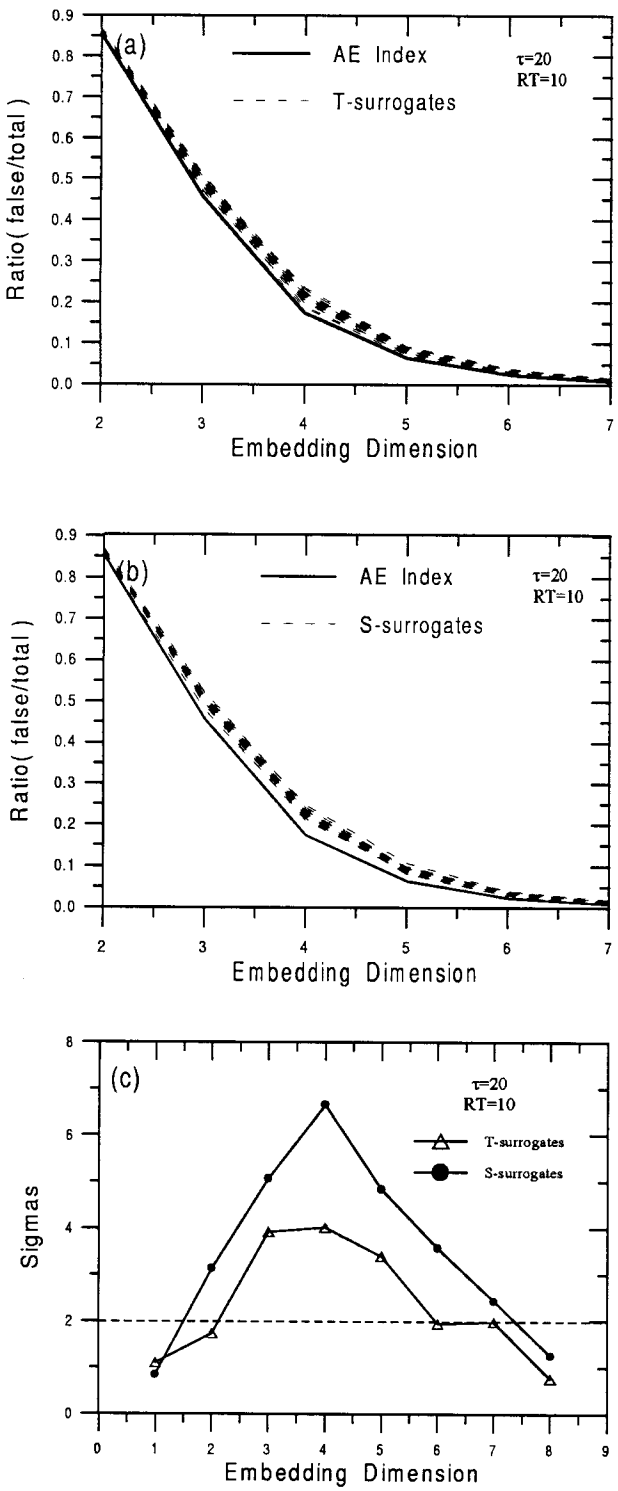

Fig. 12. (a) The ratio of the false to the total nearest neighbors for the T-surrogate data as a function of m. For this estimation we used $\tau = 20$ and $R_T = 10$. (b) The same with (a) but for the group of S-surrogate data. (c) The significance of the statistics f_{ngb} for the T-surrogate and the S-surrogate data.

3.2.4 Cumulative distance F_{dis}

The F_{dis} defined in Eq. (11) is a global measure for the deviation of the slope segment from a given plateau. In contrast to the above parameters, this parameter is appropriate as a discriminating statistic even when the slopes of the surrogate data show significant scaling profile. Figure 11a shows the magnitude of F_{dis} as a function of the embedding dimension estimated for the AE index and the corresponding mean value of F_{dis} estimated for the 40 T-surrogate data. For this estimation we used as a plateau level for each embedding the mean value $\bar{D}$ of the local slopes of the AE index on the same $\ln(r)$-interval the best scaling was observed. It is clear that the values of F_{dis} for the AE index are significantly lower from the corresponding values for the T-surrogate data. The significance of the statistic F_{dis} shown in Fig. 11b varies in the range of 2-2.5 sigmas. Figure 11c shows the discriminating statistics of the same magnitude F_{dis} for the AE index (tall line) and the S-surrogate data (short lines) for a single estimation with $m = 20$. The S-surrogate data allow for better discrimination as the significance of F_{dis} was found to be ~ 3 sigmas. Finally, in both cases the results on F_{dis} suggest the rejection of the null hypothesis with confidence $> 95\%$.

3.2.5 False nearest neighbors f_{ngb}

The ratio of the false to total nearest neighbors f_{ngb} was estimated according to the Eqs. (5), (6) for the AE index as well as for the two sets of surrogate data. Figure 12a shows the estimated ratios for the AE index and its T-surrogate data as a function of the embedding dimension and Fig. 12b for the S-surrogate data. In both cases we observe strong difference between the values of f_{ngb} corresponding to the AE index and the values of f_{ngb} corresponding to the surrogate data, especially for embedding dimensions 3-5. The significance of the discriminating statistic of f_{ngb} for T and S surrogate data is shown in Fig. 12c. For embedding dimensions in the range 2-7, the significance is large, of order 2-4 sigmas for the T-surrogates and 2-7 sigmas for the S-surrogates. The results based on the false nearest neighbors clearly suggest the rejection of the null hypothesis.

4 Summary and discussion

In this paper we introduced five geometrical quantities of the reconstructed dynamics as the discriminating statistics in order to test for the magnetospheric AE index the more general null hypothesis corresponding to the static nonlinear distortion of linearly correlated noise, according to (Theiler et al., 1992b,a).

The maximum values of the statistical significance for the geometrical quantities obtained in this study are listed in Table 1. The signals representing the null hypothesis of nonlinear static distortion of linear stochastic data were generated by two different methods, denoted with T and S respectively. In both methods, the objective is to generate surrogate signals

Table 1. This table shows the maximum values for the T-surrogates (column 3) of the statistical significance in sigmas for five different geometrical quantities (column 1) together with the corresponding parameters (column 2). For the S-surrogates (last column), the optimized significance yields only f_{ngh}, as only one set of parameters was used for the other four quantities.

Geometrical Discriminating parameters	"Nonlinear" surrogate data		
		T-surrogates	S-surrogates
	Parameters	Sigmas	Sigmas
Slopes of the correlation integrals	$m = 20$ $\tau = 60$ $\ln(r) = 4.95$	2.10	2.88
Standard deviation of the slopes (S_{dev})	$m = 20$ $\tau = 60$ $\Delta \ln(r) = (5.87 - 6.10)$	1.93	2.63
Length of scaling (L_{scal})	$m = 20$ $\tau = 60$ $\Delta \ln(r) = (5.00 - 7.00)$	5.88	6.97
Cumulative distance (F_{dis})	$m = 20$ $\tau = 60$ $\Delta \ln(r) = (4.80 - 6.50)$	2.31	2.92
False nearest neighbors (F_{ngh})	$m = 4$ $\tau = 20$ $R_T = 10$	4.00	6.64

that mimic the original signal in terms of the amplitude distribution and the power spectrum (or equivalently with autocorrelation function). The S-surrogate data turn out to mimic better the AE time series than the T-surrogate data and give sensibly higher values for the significance of the statistics as shown in Table 1.

The amplitude distribution for the AE index is non-Gaussian. For stationary time series, as AE index was found to be, if the ergodic condition is supposed to be valid it implies the non-Gaussian character of the underlying process. Non-Gaussian processes may involve interesting nonlinear dynamics such as chaos, but can also stem from stochastic Gaussian process after a nonlinear distortion. Our findings suggest the rejection of the latter hypothesis for the AE index. With statistical confidence at the 95% level (or even higher in some cases), we could discriminate the AE index from the family of linear stochastic signals with the same amplitude distribution and power spectrum as the original time series.

The rejection of the above null hypothesis strongly supports the hypothesis of low dimensionality and nonlinearity of the deterministic component of the underlying dynamical process to the AE index. More evidence on this is given in a second paper (Part II) where the dynamical characteristics are investigated in terms of surrogate data sets.

References

Abarbanel, H. D., Brown, R., Sidorowich, J. J., and Tsirming, L. S., The analysis of observed chaotic data in physical systems, *Rev. Mod. Phys.*, *65*, 1331–1392, 1993.

Argyris, J., Andreadis, I., Pavlos, G., and Athanasiou, M., The influence of noise on the correlation dimension of chaotic attractors, *Chaos, Solitons, Fractals*, *9*, 343–361, 1998.

Baker, D. N., Klimas, A. J., McPherrron, R. L., and Bucher, J., The evolution from weak to strong geomagnetic activity: an interpretation in terms of deterministic chaos, *Geophys. Res. Lett.*, *17*, 41–44, 1990.

Broomhead, D. S. and King, G. P., Extracting qualitive dynamics from experimental data, *Physica D*, *20*, 217–236, 1986.

Casdagli, M., Jardin, D. D., Eubank, S., Farmer, J. D., Gibson, J., Hunter, N., and Theiler, J., Non linear modeling of chaotic time series: Theory and applications, in *Applied Chaos*, edited by II. Kim and J. Stringer, chap. 15, pp. 335–380, John Wiley and & Sons, 1992.

Davis, T. N. and Sugiura, M., Auroral electrojet activity index ae and its universal time variation, *J. Geophys. Res.*, *71(3)*, 785–801, 1966.

Ding, M., Grebogi, C., Ott, E., Sauer, T., and York, J. A., Estimating correlation dimension from a chaotic time series: when does a plateau onset occur?, *Physica D*, *69*, 404–424, 1993.

Eckmann, J. P. and Ruelle, D., Ergodic theory of chaos and strange attractors, *Rev. Mod. Phys.*, *57*, 617–628, 1985.

Klimas, A. J., Baker, D. N., Roberts, D. A., Fairfield, D. H., and Buchner, J. A., A nonlinear dynamical analogue model of substorms, in *Magnetospheric Substorms*, edited by J. R. Kan, T. A. Potemra, S. Kokubun, and T. Iijima, pp. 449–459, AGU, Washington, D.C., 1991.

Klimas, A. J., Vassiliadis, D., Baker, D. N., and Roberts, D. A., The organized nonlinear dynamics of the magnetosphere, *Geophys. Res.*, *101*, 13 089–13 113, 1996.

Kugiumtzis, D., State space reconstruction parameters in the analysis of chaotic time series-the role of the time window length, *Physica D*, *95*, 13–28, 1996.

McPherron, R. L., Magnetospheric dynamics, in *Introduction to space physics*, edited by M. G. Kivelson and C. T. Russell, pp. 400 – 458, Cambridge University Press, 1995.

Osborne, A. R. and Provenzale, A., Finite correlation dimension for stochastic systems with power-low spectra, *Physica D*, *35*, 357–381, 1989.

Packard, N. H., Crutchfield, J. P., Farmer, J. D., and Shaw, R. S., Geometry from a time series, *Phys. Rev. Lett.*, *45*, 712–716, 1980.

Pavlos, G. P., Magnetospheric dynamics, in *Symposioum on Solar and Space Physics*, edited by D. Dialetis, pp. 1–43, National Observatory of Athens, 1988.

Pavlos, G. P., Kyriakou, G. A., Rigas, A. G., Liatsis, P. I., Trochoutos, P. C., and Tsonis, A. A., Evidence for strange attractor structures in space plasmas, *Ann. Geophys.*, *10*, 309–322, 1992a.

Pavlos, G. P., Rigas, A. G., Dialetis, D., Sarris, E. T., Karakatsanis, L. P., and Tsonis, A. A., Evidence for chaotic dynamics in outer solar plasma and the earth magnetopause, in *Chaotic Dynamics: Theory and Practice*, edited by A. Bountis, pp. 327–339, Plenum, New York, 1992b.

Pavlos, G. P., Diamadidis, D., Adamopoulos, A., Rigas, A. G., Daglis, I. A.,

and Sarris, E. T., Chaos and magnetospheric dynamics, *Nonlin. Proc. Geophys.*, *1*, 124–135, 1994.

Pavlos, G. P., Athanasiou, M. A., Diamantidis, D., Rigas, A. G., and Sarris, E. T., Comments and new results about the magnetospheric chaos hypothesis, accepted for publication in Nonlin. Proc. Geophys., 1999.

Price, C. P. and Prichard, D. J., The non-linear response of the magnetosphere: 30 october 1978, *Geophys. Res. Lett.*, *20*, 771–774, 1993.

Price, C. P., Prichard, D., and Bischoff, J. E., Nonlinear input-output analysis of the auroral electrojet index, *J. Geophys. Res.*, *99*, 13 227–13 238, 1994.

Prichard, D. and Price, C. P., Is the ae index the result of nonlinear dynamics?, *Geophys. Res. Lett.*, *20*, 2817–2820, 1993.

Prichard, D. J., Short comment for magnmetospheric chaos, *Nonlinear Proc. Geophys.*, *20*, 771–774, 1994.

Provenzale, A., Osborne, A. R., Jr., A. D. K., and Bergamasco, L., The study of fluid parcel trajectories in large-scale ocean flows, in *Nonlinear Topics in Ocean Physics*, edited by A. R. Osborns, vol. 64, pp. 367–402, Elsevier, Paris, 1991.

Ruelle, L. H. and Takens, F., On the nature of turbulence, *Commun. Math. Phys.*, *20*, 167–192, 1971.

Schreiber, T. and Schmitz, A., Improved surrogate data for nonlinearity test, *Phys. Rev. Lett.*, *77*, 635–638, 1996.

Shan, H., Hansen, P., Goertz, C. K., and Smith, K. A., Chaotic appearance of the ae index, *Geophys. Res. Lett.*, *18*, 147–150, 1991.

Takalo, J. and Timonen, J., Properties of ae data and bicolored noise, *J. Geophys. Res.*, *99*, 13 239–13 249, 1994.

Takens, F., Detecting strange attractors in turbulence, in *Lectures Notes in Mathematics*, edited by D. A. Rand and L. S. Young, vol. 898, pp. 366–381, Springer, Berlin, 1981.

Theiler, J., Some comments on the correlations dimensions of 1/f a noise, *Phys. Lett. A*, *155*, 480–493, 1991.

Theiler, J., Eubank, S., Longtin, A., Galdikian, B., and Farmer, J. D., Testing for nonlinearity in time series: the method of surrogate data, *Physica D*, *58*, 77–94, 1992a.

Theiler, J., Galdikian, B., Longtin, A., Eubank, S., and Farmer, J. D., Using surrogate data to detect nonlinearity in time series, in *Nonlinear Modeling and Forecasting*, edited by M. Casdagli and S. Eubank, vol. XII of *SFI studies in the Sciences of Complexity*, pp. 163–168, Addison-Wesley, Reading, Mass., 1992b.

Vassiliadis, D., Sharma, A. S., Eastman, T. E., and Papadopoulos, K., Low-dimensional chaos in magnetospheric activity from ae time series, *Geophys. Res. Lett.*, *17*, 1841–1844, 1990.

Vassiliadis, D., Sharma, A. S., and Papadopoulos, K., Time series analysis of magnetospheric activity using nonlinear dynamical methods, in *Chaotic Dynamics: Theory and Practice*, edited by A. Bountis, Plenum, New York, 1992.

Whitney, H., Differential manifolds, *Ann. Math.*, *37*, 645–660, 1936.